Quantum expression for the electrical conductivity of massless quark matter and of the hadron resonance gas in the presence of a magnetic field

Jayanta Dey [1,*] Subhasis Samanta,[2] Sabyasachi Ghosh,[3] and Sarthak Satapathy[4]
[1]*National Institute of Science Education and Research (NISER), Jatni 752050, Odisha, India*
[2]*Institute of Physics, Jan Kochanowski University, 25-406 Kielce, Poland*
[3]*Indian Institute of Technology Bhilai, GEC Campus, Sejbahar, Raipur 492015, Chhattisgarh, India*
[4]*Dinabandhu Mahavidyalay, North 24 Parganas, Bongaon 743235, West Bengal, India*

(Received 14 June 2022; accepted 6 October 2022; published 31 October 2022)

We have studied the classical and quantum expressions of electrical conductivity and their numerical estimation in the presence of a magnetic field for hadron resonance gas (HRG) and massless quark matter. Classical results of transport coefficients of HRG matter in the presence of a magnetic field were studied previously by Dash *et al.* [Phys. Rev. D **102**, 016016 (2020)] using the standard relaxation time approximation in the Boltzmann equation. In the same reference, the transition from isotropic transport coefficients to anisotropic coefficients in the presence of a magnetic field was also estimated for massless and HRG matter. This led to an upper limit or Stefan-Boltzmann (SB) type limit to the nonperturbative domain transition of transport coefficients. In a similar context, the present work has concentrated on the classical to quantum transition of HRG transport from the domain of high temperature and low magnetic field to that of low temperature and high magnetic field. We have also compared the quantum modification of HRG results with that of massless quark matter, where we observed an opposite trend. A similar kind of quantum effect is also noticed between mesons and baryons due to their different particle distribution functions. Despite the fact that HRG contains both mesons and baryons, Landau quantization of its net magnetothermodynamic phase space reveals meson- or boson-dominated quantum modification. That is why the quantum modification of HRG results reveals the opposite trend from that of massless quark matter, which faces fermionic quantum modification.

DOI: 10.1103/PhysRevC.106.044914

I. INTRODUCTION

In the presence of a magnetic field, quark gluon plasma (QGP) exhibits a number of interesting phenomena [1–6]. The magnitude of magnetic field produced at the BNL Relativistic Heavy Ion Collider (RHIC) for Au-Au collisions at $\sqrt{s} = 200$ GeV is of the order of 10^{19} G, and it it $eB \approx 10^{20}$ G for Pb-Pb collisions at the CERN Large Hadron Collider (LHC). This is much larger than $\Lambda_{\rm QCD}^2 (\approx 2 \times 10^{18}$ G), where $\Lambda_{\rm QCD} (\approx 0.2$ GeV) is the strong interaction scale. The magnitude of the produced field is also very high compared to those of neutron stars and magnetars, which are of the order of 10^{14}–10^{15} Gauss [7].

Understanding of the impact of this high magnetic field on different transport coefficients of QGP has recently appeared to become an important research topic within the community of heavy ion physics. Recent Refs. [8–37] have gone through the calculations of different transport coefficients such as shear viscosity [8–18], bulk viscosity [20–24], and electrical conductivity [13–15,17,25–37] in the presence of a magnetic field. Among them, electrical conductivity (σ) plays an important role in the lifetime of the magnetic field produced in heavy ion collisions (HICs). The produced magnetic field can exist for a longer time when the electrical conductivity of RHIC or LHC matter is high [38].

From microscopic calculations, studied in earlier Refs. [13–15,17,25–37], we can get temperature and magnetic field dependent values of the electrical conductivity of RHIC or LHC matter. If we analyze those investigations minutely, we can find mainly two classes of calculations: those done in classical and those done in quantum pictures. Among Refs. [13–15,17,25–29,31–37], Refs. [13–15,17,26,29,31,33,35,36] examined the classical expressions of electrical conductivity, whose multicomponent values show an anisotropy in coordinate space. They did not, however, take into account the quantum aspects of Landau quantization. In the context of neutron stars, Ref. [29] used a similar classical expression of conductivity for magnetic fields of the order of 10^{14} G, beyond which it is important to take into account the quantum effects, as done in Ref. [39]. In the quantum domain, due to the Landau quantization, the motion of charged particles gets quantized in the plane perpendicular to the magnetic field. References [25,27,28,32,34,37] considered this Landau quantization, and most of them [25,27,28,32] went through the lowest Landau level (LLL) approximation that is applicable for the strong field limit. The LLL approximation reduces the multicomponent structure of conductivity to a single component which is parallel to the magnetic field's direction.

[*]Presently at Indian Institute of Technology Indore.

This component is referred to as longitudinal conductivity. The classical framework will be useful in the weak field range, while the LLL approximated quantum framework will be useful in the strong field limit. How does the multicomponent classical expression of conductivity change during the weak to strong field transition? Answering this question is attempted in the current work using the numerical benchmark of the ideal hadron resonance gas (HRG) model, which is well established as an alternative description of QCD thermodynamics within the hadronic temperature range [40].

Using the HRG model, Refs. [15,17,33] estimated the classical multicomponent transport coefficients in the presence of a magnetic field. However, their quantum extensions have not been done yet. The current work will fill the gap by focusing solely on electrical conductivity, because the mathematical extension of other transport coefficients is analogous.

The article is organized as follows: The next section (Sec. II) addresses all working formulas of multicomponents of conductivity at a finite magnetic field with a quick description of kinetic theory formalism based on the standard relaxation time approximation (RTA). This formalism section is divided into three subsections, where Sec. II A is devoted to the expressions of anisotropic conductivity components, which we call classical expressions, then in Sec. II B, their quantum extensions are addressed. After that, in Sec. II C, HRG versions of both classical and quantum expressions are addressed; they behave as working formulas of the Results section, i.e., Sec. III. In the Results section, the classical to quantum transitions for the HRG model are graphically sketched and discussed. At the end, the investigation is summarized in Sec. IV.

II. FORMALISM

Here, we will go over the formalism section step by step so that we can see how the expressions change from classical to quantum and then to the HRG model. We know that in the presence of a magnetic field, the conductivity tensors lose their isotropic nature, and we get different numerical values or expressions for the parallel and perpendicular components and another component called the Hall conductivity. The anisotropic conductivity tensor can obtained using the relaxation time approximation (RTA) based kinetic theory approach [13,29,41], whose expressions are considered here as classical (CL) expressions where the Landau quantization is not taken into account. We are, however, considering quantum aspects of statistical mechanics by employing Fermi-Dirac (FD) and Bose-Einstein (BE) distribution functions for baryons and mesons, respectively. So, from the same perspective, the notation CL does not exactly mean classical expression. The derivation of these CL expressions is given in the following subsection (Sec. II A) and the quantum (QM) expressions, where the Landau quantization is considered, are addressed in the subsequent subsection (Sec. II B). Finally, in Sec. II C, the HRG versions of CL and QM expressions are formulated.

A. Classical expressions of electrical conductivity

For a detailed derivation of classical expressions (CL) of anisotropic conductivity reader can go through Refs. [13,14,29,41]. However, for the sake of completeness, let us quickly go through the steps of the derivation.

Let us consider an electric field $\boldsymbol{E} = E_x\hat{x}$ that is applied to a relativistic charged fermion/boson fluid, for which a current density is obtained along the same direction $\boldsymbol{J} = J_x\hat{x}$. Hence, macroscopic Ohm's law can be written as

$$J_x = \sigma_{xx}E_x, \tag{1}$$

where σ_{xx} is the electrical conductivity. In microscopic theory of dissipation, the equilibrium distribution function of fermions/bosons,

$$f_0 = \frac{1}{e^{\beta\omega} \mp 1}, \tag{2}$$

undergoes a small deviation (δf) driven by the electric field (neglecting other dissipative forces). So, the ansatz of δf can be written as

$$\begin{aligned}\delta f &\propto \left(\frac{\partial f_0}{\partial \omega}\right)\\ \delta f &= -\boldsymbol{\alpha}\cdot\boldsymbol{E}\left(\frac{\partial f_0}{\partial \omega}\right)\\ &= (\alpha_x E_x)\beta f_0(1 \mp f_0),\end{aligned} \tag{3}$$

where $\boldsymbol{\alpha}$ is an unknown coefficient that can be find using the Boltzmann transport equation. Therefore, one can express (dissipative) current density as [13,14,29,41]

$$\begin{aligned}J_x &= g\tilde{e}\int \frac{d^3\boldsymbol{k}}{(2\pi)^3}\frac{k_x}{\omega}\delta f\\ &= \left[g\tilde{e}\beta\int \frac{d^3\boldsymbol{k}}{(2\pi)^3}\frac{k_x}{\omega}\alpha_x f_0(1 \mp f_0)\right]E_x,\end{aligned} \tag{4}$$

where g is the degeneracy factor (excluding charge-flavor degeneracy), $\tilde{e}$ is electric charge, and $\omega = \{\boldsymbol{k}^2 + m^2\}^{1/2}$ is energy of the particle. To find out α_x, we take help of relaxation time approximated relativistic Boltzmann equation (RTA-RBE),

$$\begin{aligned}-\tilde{e}\boldsymbol{E}\cdot\nabla_k f_0 &= -\delta f/\tau_c\\ \Rightarrow \delta f &= \tau_c\tilde{e}\boldsymbol{E}\cdot\frac{\boldsymbol{k}}{\omega}\left[\frac{\partial f_0}{\partial \omega}\right]\\ &= \tau_c\tilde{e}E_x\left(\frac{k_x}{\omega}\right)[\beta f_0(1 \mp f_0)],\end{aligned} \tag{5}$$

where τ_c is called the relaxation time. Now, comparing Eq. (5) and (3), we get

$$\alpha_x = \tilde{e}\tau_c\frac{k_x}{\omega}. \tag{6}$$

Using the above expression of α_x in Eq. (4) and comparing with Eq. (1), we get the expression of electrical conductivity which gives rise to electric current in the x direction as

$$\sigma_{xx} = g\tilde{e}^2\beta\int \frac{d^3\boldsymbol{k}}{(2\pi)^3}\tau_c\frac{k_x^2}{\omega^2}f_0(1 \mp f_0). \tag{7}$$

Next, we will derive the electrical conductivity in the presence of a magnetic field $\boldsymbol{B} = B\hat{z}$, where the force term $\frac{d\boldsymbol{k}}{dt}$ in RTA-RBE will be modified by the Lorentz force $[-\tilde{e}(\boldsymbol{E} + \boldsymbol{v} \times \boldsymbol{B})]$ as

$$-\tilde{e}\left(\boldsymbol{E} + \frac{\boldsymbol{k}}{\omega} \times \boldsymbol{B}\right) \cdot \nabla_k f_0 = \frac{-\delta f}{\tau_c}$$
$$-\tilde{e}\left(\boldsymbol{E} + \frac{\boldsymbol{k}}{\omega} \times \boldsymbol{B}\right) \cdot \left(\frac{\boldsymbol{k}}{\omega}\right)\frac{\partial f_0}{\partial \omega} = \frac{-\delta f}{\tau_c}. \quad (8)$$

The second term on the left hand side gives null contribution because of the vector identity $(\boldsymbol{k} \times \boldsymbol{B}) \cdot \boldsymbol{k} = \boldsymbol{B} \cdot (\boldsymbol{k} \times \boldsymbol{k}) = 0$, so we consider the contribution from the term $\nabla_k(\delta f)$ in RTA-RBE,

$$-\tilde{e}\boldsymbol{E} \cdot \left(\frac{\boldsymbol{k}}{\omega}\right)\frac{\partial f_0}{\partial \omega} - \tilde{e}\left(\frac{\boldsymbol{k}}{\omega} \times \boldsymbol{B}\right) \cdot \nabla_k(\delta f) = -\delta f/\tau_c. \quad (9)$$

Here, the dissipation is driven by $\boldsymbol{E}$ as well as $\boldsymbol{B}$. So, we consider $\delta f = -(\boldsymbol{k} \cdot \boldsymbol{F})\frac{\partial f_0}{\partial \omega}$, $\boldsymbol{F}$ is a function of $\boldsymbol{E}$ and $\boldsymbol{B}$. Now, using the standard vector identity

$$\left(\frac{\boldsymbol{k}}{\omega} \times \boldsymbol{B}\right) \cdot \nabla_k(\delta f) = -\left(\frac{\boldsymbol{k}}{\omega} \times \boldsymbol{B}\right) \cdot \nabla_k(\boldsymbol{k} \cdot \boldsymbol{F})\frac{\partial f_0}{\partial \omega}$$
$$= -\left(\frac{\boldsymbol{k}}{\omega} \times \boldsymbol{B}\right) \cdot \boldsymbol{F}\frac{\partial f_0}{\partial \omega}$$
$$= -\frac{\boldsymbol{k}}{\omega} \cdot (\boldsymbol{B} \times \boldsymbol{F})\frac{\partial f_0}{\partial \omega} \quad (10)$$

in Eq. (9), we get

$$\left(\frac{\boldsymbol{k}}{\omega}\right) \cdot [-\tilde{e}\boldsymbol{E} + \tilde{e}(\boldsymbol{B} \times \boldsymbol{F})] = \boldsymbol{k} \cdot \boldsymbol{F}/\tau_c. \quad (11)$$

In general, we can consider

$$\boldsymbol{F} = [A_x\hat{x} + A_z\hat{z} + A_y(\hat{x} \times \hat{z})], \quad (12)$$

for which Eq. (11) becomes

$$\frac{\tau_c}{\omega}[-\tilde{e}E_x\hat{x} + \tilde{e}B\hat{z} \times (A_x\hat{x} + A_z\hat{z} - A_y\hat{y})]$$
$$= (A_x\hat{x} + A_z\hat{z} - A_y\hat{y}). \quad (13)$$

Equating the coefficients of $\hat{x}$, $\hat{z}$ and $\hat{y}$ of Eq. (13), we get

$$A_z = 0,$$
$$A_x = -\tilde{e}\frac{1}{1 + (\tau_c/\tau_B)^2}\frac{\tau_c}{\omega}E_x,$$
$$A_y = \tilde{e}\frac{\tau_c/\tau_B}{1 + (\tau_c/\tau_B)^2}\frac{\tau_c}{\omega}E_x, \quad (14)$$

where $\tau_B = \omega/(\tilde{e}B)$ is the inverse of cyclotron frequency. So, the final form of the deviation becomes

$$\delta f = -\boldsymbol{k} \cdot \left\{-\frac{\tilde{e}\tau_c}{\omega}\left(\hat{x} + \frac{\tau_c}{\tau_B}\hat{y}\right)\right\}\frac{1}{1 + (\tau_c/\tau_B)^2}\frac{\partial f_0}{\partial \omega}$$
$$= -\tilde{e}\tau_c\left(\frac{k_x}{\omega} + \frac{k_y}{\omega}\frac{\tau_c}{\tau_B}\right)E_x\frac{1}{1 + (\tau_c/\tau_B)^2}\beta f_0(1 - f_0). \quad (15)$$

Now, using this δf in the matrix form of Ohm's law,

$$\begin{pmatrix} J_x \\ J_y \end{pmatrix} = \begin{pmatrix} \sigma_{xx} & \sigma_{xy} \\ \sigma_{yx} & \sigma_{yy} \end{pmatrix}\begin{pmatrix} E_x \\ 0 \end{pmatrix}, \quad (16)$$

one can obtain

$$\sigma_{xx} = g\tilde{e}^2\beta\int\frac{d^3\boldsymbol{k}}{(2\pi)^3}\tau_c\frac{1}{1 + (\tau_c/\tau_B)^2}\frac{k_x^2}{\omega^2}f_0(1 \mp f_0)$$
$$= g\tilde{e}^2\beta\int\frac{d^3\boldsymbol{k}}{(2\pi)^3}\tau_c\frac{1}{1 + (\tau_c/\tau_B)^2}\frac{\boldsymbol{k}^2}{3\omega^2}f_0(1 \mp f_0), \quad (17)$$
$$\sigma_{yx} = g\tilde{e}^2\beta\int\frac{d^3\boldsymbol{k}}{(2\pi)^3}\tau_c\frac{\tau_c/\tau_B}{1 + (\tau_c/\tau_B)^2}\frac{k_y^2}{\omega^2}f_0(1 \mp f_0)$$
$$= g\tilde{e}^2\beta\int\frac{d^3\boldsymbol{k}}{(2\pi)^3}\tau_c\frac{\tau_c/\tau_B}{1 + (\tau_c/\tau_B)^2}\frac{\boldsymbol{k}^2}{3\omega^2}f_0(1 \mp f_0), \quad (18)$$

where $g\tilde{e}^2 = 2 \times 2 \times 3(\frac{4e^2}{9} + \frac{e^2}{9} + \frac{e^2}{9}) = 8e^2$ for three-flavor quark matter [14,34]. For other relevant system or matter (e.g., HRG matter), we have to consider corresponding $g\tilde{e}^2$ values.

Similarly, σ_{yy}, σ_{xy} can be obtained by repeating the same calculation for $\boldsymbol{E} = E_y\hat{y}$, and they are related as $\sigma_{xx} = \sigma_{yy}$, $\sigma_{xy} = -\sigma_{yx}$. Longitudinal conductivity along z-axis will remain unaffected by the magnetic field, because the Lorentz force does not work along the direction of the magnetic field. Hence, the classical expression of the longitudinal conductivity will be

$$\sigma_{zz} = g\tilde{e}^2\beta\int\frac{d^3\boldsymbol{k}}{(2\pi)^3}\tau_c\frac{k_z^2}{\omega^2}f_0(1 \mp f_0)$$
$$= g\tilde{e}^2\beta\int\frac{d^3\boldsymbol{k}}{(2\pi)^3}\tau_c\frac{\boldsymbol{k}^2}{3\omega^2}f_0(1 \mp f_0), \quad (19)$$

For particle and antiparticle cases, the term τ_c/τ_B in the numerator for the Hall component, $\sigma_\times = \sigma_{xy} = -\sigma_{yx}$, has the opposite sign, resulting in vanishing net Hall conductivity at the vanishing quark/baryon chemical potential ($\mu = 0$). Here, however, this fact may be difficult to see when looking at the Eq. (18), because the particle-antiparticle contribution is included in the degeneracy factor g rather than the sum of their contributions. So, for the Hall conductivity expression (18), we have to add particle and antiparticle contributions separately instead of considering two factors for particle-antiparticle degeneracy. Here, we will concentrate on the parallel component $\sigma_\parallel = \sigma_{xx} = \sigma_{yy}$ and the perpendicular component $\sigma_\perp = \sigma_{zz}$ because our current focus is on conductivity components of RHIC or LHC matter with almost zero quark/baryon chemical potential, where the Hall component vanishes.

B. Quantum expressions of electrical conductivity

Here, we will consider the effect of Landau quantization on the conductivity and see how it differs from CL expressions. The main modification will occur in the dispersion relation and the phase space integration. As we considered the magnetic field in the z direction, momentum quantization will occur in the perpendicular plane, i.e., x-y plane. The mathematical modifications will be as follows:

$$\omega = (\boldsymbol{k}^2 + m^2)^{1/2} \rightarrow \omega_l = \left(k_z^2 + m^2 + 2l|\tilde{e}|B\right)^{1/2}, \quad (20)$$

$$2\int\frac{d^3\boldsymbol{k}}{(2\pi)^3} \rightarrow \sum_{l=0}^{\infty}\alpha_l\frac{|\tilde{e}|B}{2\pi}\int_{-\infty}^{+\infty}\frac{dk_z}{2\pi}, \quad (21)$$

where spin degeneracy 2 in the left-hand side of the last line will be converted to α_l, which will be 2 for all Landau levels l, except the lowest Landau level (LLL) $l = 0$, where $\alpha_l = 1$. In general, one can write $\alpha_l = 2 - \delta_{l,0}$. Here, we also assume, roughly, $k_x^2 \approx k_y^2 \approx (\frac{k_x^2+k_y^2}{2}) = \frac{2l\tilde{e}B}{2}$; then conductivities can be expressed as

$$\sigma^{xx} = g\tilde{e}^2\beta \sum_{l=0}^{\infty} \alpha_l \frac{|\tilde{e}|B}{2\pi} \int_{-\infty}^{+\infty} \frac{dk_z}{2\pi} \frac{l|\tilde{e}|B}{\omega_l^2} \tau_c \times \frac{1}{1+(\tau_c/\tau_B)^2} f_0(\omega_l)[1 - f_0(\omega_l)],$$

$$\sigma^{zz} = g\tilde{e}^2\beta \sum_{l=0}^{\infty} \alpha_l \frac{|\tilde{e}|B}{2\pi} \int_{-\infty}^{+\infty} \frac{dk_z}{2\pi} \frac{k_z^2}{\omega_l^2} \tau_c \times f_0(\omega_l)[1 - f_0(\omega_l)]. \quad (22)$$

Most previous works on Landau quantization [25,27,28,32] considered only longitudinal conductivity σ^{zz} for $l = 0$, known as the LLL approximation. At extremely high magnetic fields, this scenario could be realized, in which all medium constituents occupy the lowest energy level $l = 0$. It means that perpendicular motion of medium constituents completely disappears as $k_x \approx k_y \approx 0$ at $l = 0$. Therefore, in this LLL case, $\sigma^{xx} \approx \sigma^{xy} \approx 0$ and $\sigma^{zz} \neq 0$. However, below such strong magnetic fields, $l > 0$ energy levels might have some non-negligible contributions, and the LLL approximation is not sufficient enough.

C. Classical and quantum expression of electrical conductivity under the hadron resonance gas model

Now we will look at the HRG model calculation and see the transition from classical to quantum. The massless case is a noninteracting or Stefan-Boltzmann (SB) limit type case, whereas HRG calculation maps the interacting picture. Neutral hadrons do not have any role in electrical conductivity. So, for the conductivity calculation, we can classify hadrons into

(1) charged mesons (M), which are basically bosons,
(2) charged baryons (B), which are basically fermions.

The contributions from both types of hadron will be added up. Under the HRG model, the classical equations (17) and (19) for perpendicular and parallel components of electrical conductivity will be modified to

$$\sigma^{xx} = \sum_{M,B} g\tilde{e}^2\beta \int \frac{d^3\boldsymbol{k}}{(2\pi)^3} \tau_c \frac{1}{1+(\tau_c/\tau_B)^2} \frac{\boldsymbol{k}^2}{3\omega^2} f_0(1 \pm f_0), \quad (23)$$

$$\sigma^{zz} = \sum_{M,B} g\tilde{e}^2\beta \int \frac{d^3\boldsymbol{k}}{(2\pi)^3} \tau_c \frac{\boldsymbol{k}^2}{3\omega^2} f_0(1 \pm f_0). \quad (24)$$

Similarly, the quantum expressions (22) will be modified as

$$\sigma^{xx} = \sum_{M} g\tilde{e}^2\beta \left(\frac{|\tilde{e}|B}{2\pi}\right) \sum_{l=0}^{\infty} \alpha_l \int_{-\infty}^{+\infty} \frac{dk_z}{2\pi} \frac{(l+1/2)|\tilde{e}|B}{\omega_l^2} \tau_c \times \frac{1}{1+(\tau_c/\tau_B)^2} f_0(\omega_l)[1 + f_0(\omega_l)] + \sum_{B} g\tilde{e}^2\beta \left(\frac{|\tilde{e}|B}{2\pi}\right) \sum_{l=0}^{\infty} \alpha_l \int_{-\infty}^{+\infty} \frac{dk_z}{2\pi} \frac{l|\tilde{e}|B}{\omega_l^2} \tau_c \times \frac{1}{1+(\tau_c/\tau_B)^2} f_0(\omega_l)[1 - f_0(\omega_l)], \quad (25)$$

$$\sigma^{zz} = \sum_{M} g\tilde{e}^2\beta \left(\frac{|\tilde{e}|B}{2\pi}\right) \sum_{l=0}^{\infty} \alpha_l \times \int_{-\infty}^{+\infty} \frac{dk_z}{2\pi} \frac{k_z^2}{\omega_l^2} \tau_c f_0(\omega_l)[1 + f_0(\omega_l)] + \sum_{B} g\tilde{e}^2\beta \left(\frac{|\tilde{e}|B}{2\pi}\right) \sum_{l=0}^{\infty} \alpha_l \times \int_{-\infty}^{+\infty} \frac{dk_z}{2\pi} \frac{k_z^2}{\omega_l^2} \tau_c f_0(\omega_l)[1 - f_0(\omega_l)]. \quad (26)$$

We have tabulated the expression of ω_l and α_l for various particle species with their corresponding spin in Table I [42,43]. For the sake of simplicity, we only considered mesons with spin 0 and 1, as well as baryons with spin 1/2 and 3/2. Higher spin hadrons are not considered, which may be justified given their low thermodynamic weight factors due to their large masses.

Since baryons are fermions, their perpendicular momenta are $k_x^2 \approx k_y^2 \approx (\frac{k_x^2+k_y^2}{2}) = \frac{2l\tilde{e}B}{2}$, whereas for the mesons perpendicular momenta are $k_x^2 \approx k_y^2 \approx (\frac{k_x^2+k_y^2}{2}) = \frac{(2l+1)\tilde{e}B}{2}$. As a result, there will be an interesting difference between massless quark matter and HRG systems. The perpendicular component will vanish for quark matter but not for HRG systems because of nonzero contribution from the charged mesons in the LLL case. This fact will be illustrated graphically in the result section.

Here, for the HRG system, we have to take care of the factors $g\tilde{e}^2$ for different hadrons; they are basically multiplication of degeneracy factor g and the square of their electric charge $\tilde{e}^2$. For example, a π^+ meson with mass 140 MeV, spin 0 has $g\tilde{e}^2 = 1 \times e^2$; a ρ^+ meson with mass 770 MeV, spin 1 has $g\tilde{e}^2 = 3 \times e^2$; a Δ^{++} baryon with mass 1232 MeV, spin 3/2 has $g\tilde{e}^2 = 4 \times 4e^2$, etc.

III. RESULTS

Let us begin with massless quark matter, which can be considered as noninteracting or Stefan-Boltzmann (SB) limit type estimations. We will not consider the gluons because they do not participate in conductivity. Massless quark matter entails taking into account all degeneracy factors: three for color degeneracy, 2 for spin degeneracy, two for particle antiparticle degeneracy, and two for flavor degeneracy

TABLE I. Particle energy and degeneracy.

Particle species	Spin	ω_l	α_l
Baryon	1/2	$\omega_l = (k_z^2 + m^2 + 2l\lvert\tilde{e}\rvert B)^{1/2}$	$2 - \delta_{l0}$
Baryon	3/2	$\omega_l = (k_z^2 + m^2 + 2l\lvert\tilde{e}\rvert B)^{1/2}$	$4 - 2\delta_{l0} - \delta_{l1}$
Meson	0	$\omega_l = (k_z^2 + m^2 + (2l+1)\lvert\tilde{e}\rvert B)^{1/2}$	1
Meson	1	$\omega_l = (k_z^2 + m^2 + (2l+1)\lvert\tilde{e}\rvert B)^{1/2}$	$3 - \delta_{l0}$

(with appropriate electric charge). Though massless s quark consideration, like that of massless u and d quarks, is a bit of a rough approximation, QGP can reach these massless or SB limits at very high temperature limits. Following the estimation of the massless quark matter case, we will proceed to HRG calculations, which may effectively be considered as interacting QCD estimations because their thermodynamics match with lattice QCD (LQCD) thermodynamics data within the hadronic temperature range. As massless limits of thermodynamic quantities such as pressure, energy density, and entropy density are considered reference points of the upper bound, similarly, the normalized conductivity components of massless quark matter can be used as that reference point here as well. Then, when we calculate HRG estimates of conductivity components, we will be representing their interacting estimates, which are expected to be suppressed from their massless limits within the hadronic temperature domain, just like thermodynamical quantities. Estimation of these noninteracting to interacting transformations of conductivity tensors are well discussed in Ref. [15] using the classical expressions of massless quark matter and HRG models, given in Eqs. (17), (19), and (23). However, their transition from a classical to a quantum picture has never been explored in previous works using the quantum expressions given in Eqs. (25) and (26). The purpose of this work is to investigate this fact. So, to begin, we will investigate the classical to quantum transition for massless quark matter first, followed by HRG matter. Throughout the discussion, we will attempt to visualize all transitions from massless or noninteracting pictures to HRG or interacting pictures, as well as from classical (CL) to quantum (QM) pictures.

Let us begin by looking at Figs. 1 and 2, which show CL and QM curves of conductivity components along the T and B axes, respectively. Using CL Eq. (19), parallel component of conductivity for massless quark matter will be [13]

$$\sigma_\parallel = 8e^2 \frac{\zeta(2)}{3\pi^2} \tau_c T^2, \tag{27}$$

where $\zeta(2) = \pi^2/6$. As a result, for the massless quark matter case, $\sigma_\parallel \propto \tau_c T^2$, so its normalized values $\sigma_\parallel/(\tau_c T^2)$ will be constant, as shown by the green dash-dotted horizontal line in Figs. 1 and 2, which will serve as our reference points like the SB limit for thermodynamical quantities [15,44]. Next, we will calculate the deviation from a horizontal line in the high B and low T domains using QM Eq. (22) of $\sigma_\parallel$. This fact is explored by the QM curves of $\sigma_\parallel$: grey double-dash-dotted lines in Figs. 1 and 2. This deviation increases towards the low T and high eB domains due to Landau quantization, or, in other words, due to the transition from integration to Landau level summation, as denoted in Eq. (21). The QM and CL curves of $\sigma_\parallel$, on the other hand, are merging because integration and Landau level summation become equivalent in the high T and low eB ranges. In the left panel of Fig. 10 in Ref. [44], a similar enhancement for entropy density with respect to SB limit was found in the low T domain. Therefore, the SB or massless limits of normalized entropy density (s/T^3) or other thermodynamical quantities, as well as normalized longitudinal conductivity ($\sigma_\parallel/\tau_c T^2$), exhibit the same pattern. For both cases, their horizontal lines deviate (are enhanced) in the low T domain due to Landau quantization. This Landau quantization effect is can be seen in low T and high eB domains, which is a well-known fact for all thermodynamical quantities and transport coefficients. Based on this, we can assume that low T and high eB are quantum domains whereas high T and low eB are classical domains. So, these enhanced normalized quantities (s/T^3, $\sigma_\parallel/\tau_c T^2$) of massless quark matter may be realized as an enhancement of their magnetothermodynamical phase-space in the quantum domain.

We also estimated $\sigma_\parallel/\tau_c T^2$ for the lowest Landau level (LLL) approximation by imposing $l = 0$ in Eq. (22), as shown in Figs. 1 and 2 by cyan dash-double-dotted lines. An enormous difference between the full Landau level estimation (brown double-dash-dotted lines) and the LLL approximation (cyan dash-double-dotted) is visible. As expected, they are merging into the high eB and low T domains. However, according to our graphs, this convergence of LLL approximation and actual QM estimation is unlikely within the range of RHIC/LHC matter, covering $T = 0.1$–0.4 GeV and

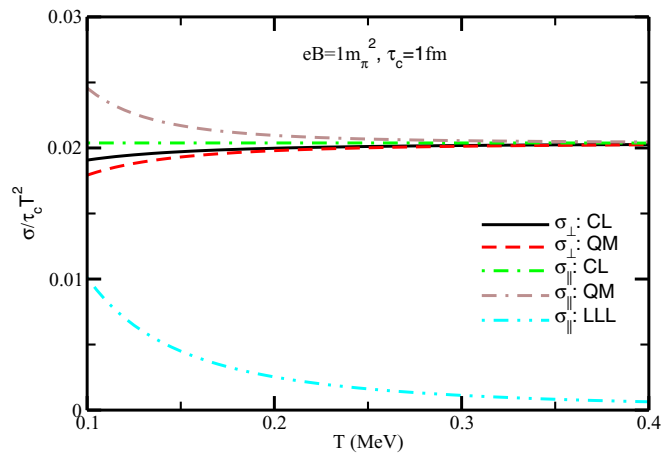

FIG. 1. Components of electrical conductivity for massless quark matter as a function of temperature.

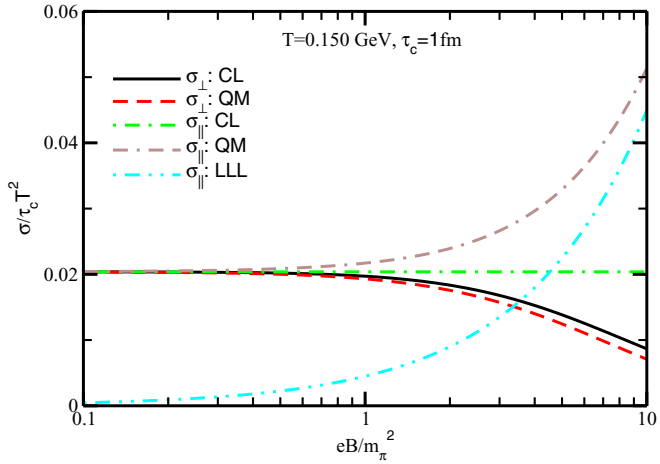

FIG. 2. Components of electrical conductivity as a function of magnetic field for massless quark matter.

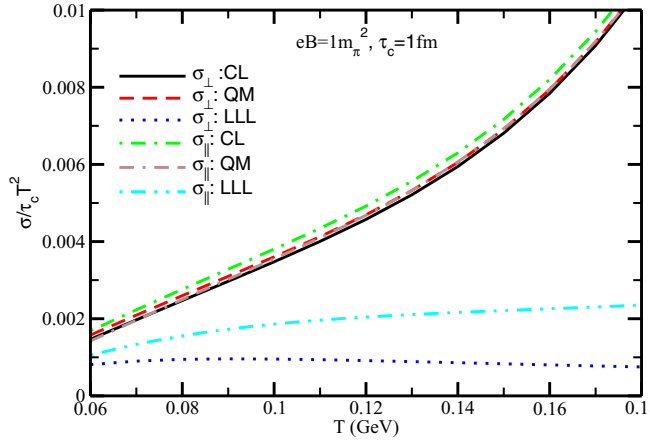

FIG. 3. Components of electrical conductivity for HRG matter as a function of temperature.

$eB = (1\text{–}10)m_\pi^2$. From Fig. 2, we can say that for massless QGP at $T = 0.150$ GeV the Landau quantization effect is noticeable beyond $eB = 1m_\pi^2$ and LLL is not a good approximation within $eB = (1\text{–}10)m_\pi^2$. As a result, neither the CL nor the LLL approximation will be valid for estimating conductivity for RHIC/LHC matter with an expected magnetic field of $eB = (1\text{–}10)m_\pi^2$. The current work is intended to convey this message.

The perpendicular conductivity $\sigma_\perp$, from Eq. (17), can be simplified for massless quark matter as

$$\sigma_\perp = 12\frac{\zeta(2)}{3\pi^2}\tau_c T^2 \sum_{f=u,d,s} \frac{e_f^2}{1+(\tau_c e_f B/3T)^2}, \qquad (28)$$

where $e_f = +\frac{2}{3}e, -\frac{1}{3}e, -\frac{1}{3}e$ for $f = u, d, s$ and average energy of massless quark is used as $3T$. To grasp the graphical nature of $\sigma_\perp$, we looked at the simple analytic form, which has an additional anisotropic factor $\frac{1}{1+(\tau_c/\tau_B)^2}$ with an average of $\tau_B = 3T/(e_f B)$. As a result, the dimensionless value of $\sigma_\perp/(\tau_c T^2)$ is an anisotropic factor that rises with T and falls with eB. The solid black lines in Figs. 1 and 2 demonstrate this fact. In comparison to the CL curves, the QM curves of $\sigma_\perp/(\tau_c T^2)$ (red dashed line) are suppressed, whereas the QM curves of $\sigma_\parallel/(\tau_c T^2)$ (brown double-dash-dotted line) are enhanced. Landau quantization of the FD distribution, in fact, always enhances probability in the quantum domain (low T and high eB), resulting in higher $\sigma_\parallel/(\tau_c T^2)$. On the other hand, $\sigma_\perp/(\tau_c T^2)$ face two opposite effects. One is Landau quantization via FD distribution, for which conductivity increases in the quantum domain, and another is the anisotropic factor, which is responsible for reducing the conductivity in the quantum domain. We notice that latter effect is more dominant and perpendicular conductivity becomes suppressed in the quantum domain.

Let us now proceed to the HRG model conductivity estimation, where all charged hadrons will be included with their respective statistical weight factors due to their different mass values. These different statistical weight factors (roughly $e^{-\beta m}$) of the FD and BE distributions will act on baryons and mesons, causing HRG estimations to remain lower than massless quark matter. According to Fig. 3, in the hadronic temperature domain $T = 0.100$–0.170 GeV, $\sigma_{\parallel,\perp}/(\tau_c T^2)$ for HRG estimation, the range is 0.003–0.01, which is significantly lower than their massless quark matter estimation (around 0.02). Similar suppression values in thermodynamical quantities are realized as nonperturbative sources of QCD in LQCD calculations, which are well mapped alternatively by the HRG model. Therefore, we can assume that Figs. 1 and 3 reflect the pQCD/massless limits and non-pQCD domains of conductivity, respectively, in the high and low temperature domains. This fact is thoroughly examined in Ref. [15] using CL expressions of the massless and HRG systems. Here, we concentrate only on its QM modification, and some interesting results are as follows. QM > CL in the low T and high eB domains for the massless case, but QM < CL for the HRG case for $\sigma_\parallel/(\tau_c T^2)$. To understand the suppressed QM values for HRG estimation, where both bosons and mesons contribute, their individual investigations will be helpful. That will be discussed later.

To understand the detailed cyclotron motions of different charged hadrons, we have calculated their average cyclotron

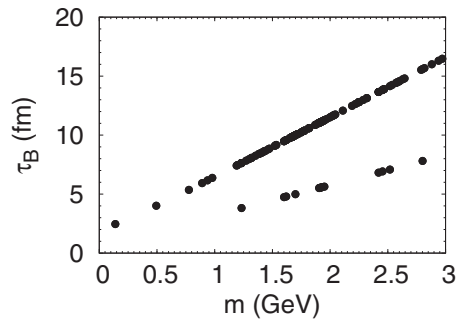

FIG. 4. Average values of inverse cyclotron frequency τ_B (in fm) for different hadrons.

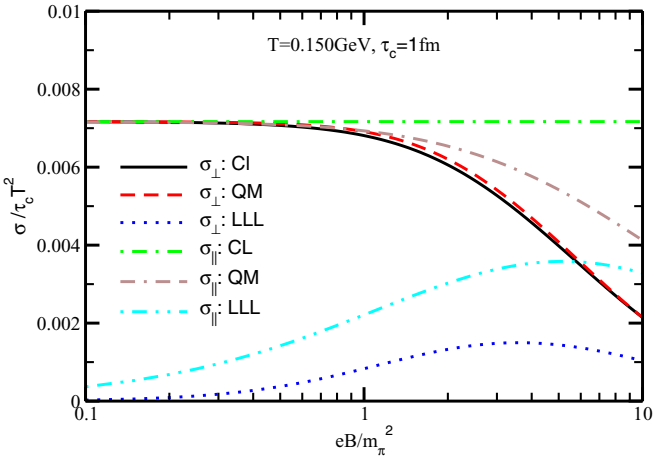

FIG. 5. Components of electrical conductivity as a function of magnetic field in the HRG model

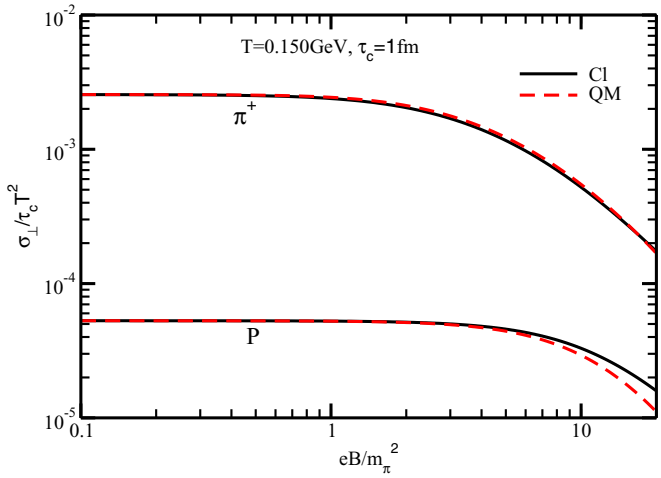

FIG. 6. Perpendicular component of electrical conductivity as a function of magnetic field for pion and proton

time period (inverse of cyclotron frequency)

$$\tau_B(m) = \frac{\omega_{\rm av}}{|\tilde{e}|B} = \frac{1}{|\tilde{e}|B}\frac{\int d^3\boldsymbol{k}\,\omega f_0(m)}{\int d^3\boldsymbol{k}\, f_0(m)}, \tag{29}$$

which is plotted against the mass (m) axis in Fig. 4. Different points represent different hadrons with their respective masses. It is obvious that τ_B will increase with m and decrease with $\tilde{e}$, as shown by the graphs. The majority of hadrons with charges $|\tilde{e}| = |e|$ lie within a specific slope of τ_B vs m, while a few deviate due to their charges $|\tilde{e}| > |e|$. As a result, higher charged, lighter mass hadrons will play an important role in the suppression of $\sigma_\perp$ via the anisotropic factor $\frac{1}{1+(\tau_c/\tau_B)^2}$.

We plotted $\sigma_\perp$ and $\sigma_\parallel$ as a function of magnetic field in Fig. 5 at $T = 0.150$ GeV and $\tau_c = 1$ fm for CL, QM, and LLL cases in the HRG system. Table II summarises the key findings by comparing the HRG estimations in Figs. 3 and 5 with massless quark matter estimations in Figs. 1 and 2. This applies to the hadronic temperature range $T \approx 0.100$–0.170 GeV with experimentally expected magnetic field range $eB \approx (0$–$10)m_\pi^2$, and is more effective in the quantum domain, i.e., low T and high eB zone. When we individually analyze proton and pion matter contributions, we can understand why massless quark matter and HRG matter outcomes are quite different from one another. These are discussed in the next paragraphs for the case of $\sigma_\parallel$ only.

The tabulated outcome indicates that the quantum effects on the pion (π) and proton (p) are exactly opposite due to their corresponding bosonic and fermionic distribution functions, respectively. Moreover, the qualitative results of HRG and pion matter are identical, which indicates that mesons dominate over baryons in the estimation of HRG. Mesons are expected to dominate in the HRG estimations due to their higher thermodynamical probabilities as a result of their low masses. Here, we explore this fact graphically for one of the components of conductivity, $\sigma_\perp$. In Fig. 6, we have plotted $\sigma_\perp/(\tau_c T^2)$ as a function of eB/m_π^2 for a pion (upper panel) and a proton (lower panel) at $T = 0.150$ GeV and $\tau_c = 1$ fm. We find that the conductivity for π^+ is much higher than that of p, which is because of the small mass of the pion. Although the QM results for the pion case (red dashed line) are larger than the CL results (black solid line), the difference is negligible. In contrast, the opposite ranking is clearly observed in the proton case. The magnetothermodynamical phase spaces of the pion and proton, which are bosons and fermions, are enhanced and suppressed, respectively, due to their (Landau) quantized BE and FD distribution functions. Figure 7 provides a detailed description of how pion and proton matter is either enhanced or suppressed in QM results compared to CL results. Here, we have plotted $(\sigma_\perp^{\rm QM} - \sigma_\perp^{\rm CI})/\sigma_\perp^{\rm QM} \times 100\%$ as a function of eB/m_π^2 for HRG (black solid line), π^+ (red dotted line), and p (blue dashed line) matter. Notice that below $eB = 1m_\pi^2$ the deviation is less than 1%. For the HRG result, deviation increases slowly with the magnetic field, reaches a maximum of $\approx$3%, and then decreases to 0% at $eB \approx 10m_\pi^2$, and further increase of magnetic field will start the suppression. Even though the CL result for the pion and proton deviates from the QM result, they follow a similar trend, and their combined effect is reflected in the HRG result. Within the magnetic field range $eB = (0$–$10)m_\pi^2$ and temperature $T = 0.150$ GeV, the contribution from mesons become larger than that of baryons, and as a result the HRG results exhibit effectively bosonic quantum modification. That is why HRG results are the opposite of those of massless quark matter, which are subjected to fermionic quantum modification.

TABLE II. Comparison between QM and CL estimations for different cases.

Medium	$\sigma_\parallel(T,B)$	$\sigma_\perp(T,B)$
Massless quark matter	QM > CL	QM < CL
HRG matter	QM < CL	QM > CL
Proton matter	QM > CL	QM < CL
Pion matter	QM < CL	QM > CL

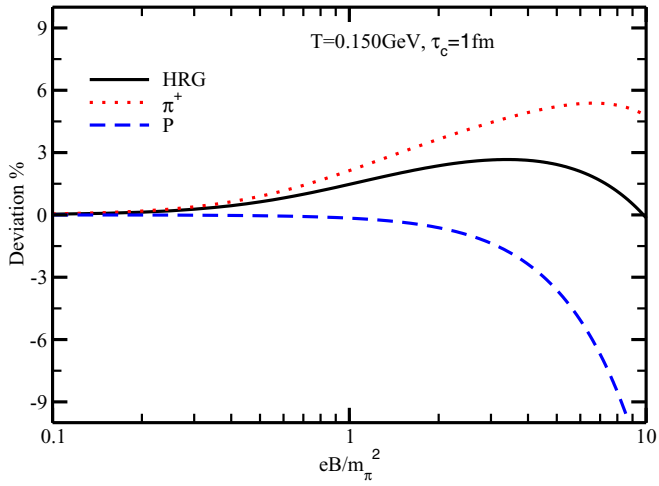

FIG. 7. Percentage deviation of classical estimation of conductivity from that of quantum estimation, as a function of magnetic field. Deviation $= (\sigma_\perp^{\rm QM} - \sigma_\perp^{\rm Cl})/\sigma_\perp^{\rm QM}$.

IV. SUMMARY

In summary, we have explored comparative estimations of classical and quantum expressions of electrical conductivity in the presence of a magnetic field. We first obtained the results for the massless quark gluon plasma, and then we used HRG model calculations to obtain the results for interacting QCD. In the presence of a magnetic field, there will be three components: parallel, perpendicular, and Hall. At zero quark/baryon chemical potential, the medium carries an equal number of opposite electrical charges, so the Hall conduction will disappear. In both classical (without considering Landau quantization) and quantum pictures, parallel and perpendicular conductivity become different in the presence of the external magnetic field. Conductivities change from being isotropic to anisotropic with a low to high magnetic field in both the CL and QM cases. In Refs. [15], the classical estimation of conductivity tensors for massless quark matter and HRG matter is thoroughly discussed. The goal of the current work is to discover their quantum extension by introducing Landau quantization. Our estimation is limited to the hadronic temperature domain $T = 0.100$–0.170 GeV and the magnetic field domain $eB = (0$–$10)m_\pi^2$. The findings are summarizedas follows:

(i) QM enhancement is observed in parallel/longitudinal conductivity for massless quark matter and proton (baryonic) matter in the presence of a magnetic field.
(ii) QM suppression is observed in perpendicular/transverse conductivity for massless quark matter and proton (baryonic) matter in the presence of a magnetic field.
(iii) QM suppression is observed in parallel/longitudinal conductivity for pionic (mesonic) matter and HRG matter in the presence of a magnetic field.
(iv) QM enhancement is observed in perpendicular/transverse conductivity for pionic (mesonic) matter and HRG matter in the presence of a magnetic field.

The QM effects in bosons and fermions are different because of their corresponding BE and FD distribution functions, which also serve to reveal the effect of Landau level summation in two different ways. Additionally, we have demonstrated that, for the ranges of temperature and magnetic field under consideration, the lowest Landau level approximation of the HRG estimation is in no way a good approximation. In the presence of a magnetic field, full Landau level summation is recommended for the quantum version of HRG estimations. Therefore, the current work, for the first time, suggests a non-negligible quantum effect in the estimation of the transport coefficient for HRG matter, which may also be applicable to other HRG-based phenomenology. In Refs. [27,37], where a quasiparticle-based model (effective fugacity quasiparticle model) was used to estimate the transport coefficients, a similar effect of Landau quantization for QGP medium was also found. The current work only considered the electrical conductivity, but we anticipate it will be applicable to other transport coefficients such as shear and bulk viscosity, thermal conductivity, as well as other HRG-related phenomenology that may be investigated in the future.

ACKNOWLEDGMENTS

S.S. acknowledges support of a fellowship funded by the DST INSPIRE Faculty Scheme of Research Project (IFA18-PH220) and thanks the principle investigator of that project (Dr. Sudipan De).

[1] J. Rafelski and B. Muller, Magnetic Splitting of Quasimolecular Electronic States in Strong Fields, Phys. Rev. Lett. **36**, 517 (1976).
[2] D. N. Voskresensky and N. Y. Anisimov, Properties of a pion condensate in a magnetic field, Sov. Phys. JETP **51**, 13 (1980).
[3] S. Schramm, B. Muller, and A. J. Schramm, Quark–anti-quark condensates in strong magnetic fields, Mod. Phys. Lett. A **07**, 973 (1992).
[4] S. Schramm, B. Muller, and A. J. Schramm, Exact Dirac propagator in a magnetic sheet, Phys. Lett. A **164**, 28 (1992).
[5] D. E. Kharzeev, L. D. McLerran, and H. J. Warringa, The Effects of topological charge change in heavy ion collisions: "Event by event $\mathcal{P}$ and $\mathcal{CP}$ violation", Nucl. Phys. A **803**, 227 (2008).
[6] D. Kharzeev, K. Landsteiner, A. Schmitt, and H. U. Yee, *Strongly Interacting Matter in Magnetic Fields*, Lecture Notes in Physics (Springer, Berlin, 2013), Vol. 871.
[7] J. H. Seiradakis and R. Wielebinski, Astron. Astrophys. Rev. **12**, 239 (2004).
[8] S. Li and H. U. Yee, Shear viscosity of the quark-gluon plasma in a weak magnetic field in perturbative QCD: Leading log, Phys. Rev. D **97**, 056024 (2018).
[9] S.-i. Nam and C.-W. Kao, Shear viscosity of quark matter at finite temperature under an external magnetic field, Phys. Rev. D **87**, 114003 (2013).

[10] A. N. Tawfik, A. M. Diab and T. M. Hussein, SU(3) Polyakov linear-sigma model: bulk and shear viscosity of QCD matter in finite magnetic field, Int. J. Adv. Res. Phys. Sci. **3**, 4 (2016).

[11] K. Tuchin, On viscous flow and azimuthal anisotropy of quark-gluon plasma in strong magnetic field, J. Phys. G: Nucl. Part. Phys. **39**, 025010 (2012).

[12] S. Ghosh, P. Mohanty, B. Chatterjee, A. Mukharjee, and H. Mishra, Impact of magnetic field on shear viscosity of quark matter in Nambu–Jona-Lasinio model, Phys. Rev. D **100**, 034024 (2019).

[13] J. Dey, S. Satapathy, P. Murmu, and S. Ghosh, Shear viscosity and electrical conductivity of the relativistic fluid in the presence of a magnetic field: A massless case, Pramana **95**, 125 (2021).

[14] J. Dey, S. Satapathy, A. Mishra, S. Paul, and S. Ghosh, From noninteracting to interacting picture of quark–gluon plasma in the presence of a magnetic field and its fluid property, Int. J. Mod. Phys. E **30**, 2150044 (2021).

[15] A. Dash, S. Samanta, J. Dey, U. Gangopadhyaya, S. Ghosh, and V. Roy, Anisotropic transport properties of a hadron resonance gas in a magnetic field, Phys. Rev. D **102**, 016016 (2020).

[16] Z. Chen, C. Greiner, A. Huang, and Z. Xu, Phys. Rev. D **101**, 056020 (2020).

[17] A. Das, H. Mishra, and R. K. Mohapatra, Transport coefficients of hot and dense hadron gas in a magnetic field: A relaxation time approach, Phys. Rev. D **100**, 114004 (2019).

[18] G. S. Denicol, X. G. Huang, E. Molnár, G. M. Monteiro, H. Niemi, J. Noronha, D. H. Rischke, and Q. Wang, Nonresistive dissipative magnetohydrodynamics from the Boltzmann equation in the 14-moment approximation, Phys. Rev. D **98**, 076009 (2018).

[19] P. Mohanty, A. Dash, and V. Roy, One particle distribution function and shear viscosity in magnetic field: a relaxation time approach, Eur. Phys. J. A **55**, 35 (2019).

[20] K. Hattori, X. G. Huang, D. H. Rischke, and D. Satow, Bulk viscosity of quark-gluon plasma in strong magnetic fields, Phys. Rev. D **96**, 094009 (2017).

[21] X. G. Huang, M. Huang, D. H. Rischke, and A. Sedrakian, Anisotropic hydrodynamics, bulk viscosities and r-modes of strange quark stars with strong magnetic fields, Phys. Rev. D **81**, 045015 (2010).

[22] N. O. Agasian, Bulk viscosity of quark-gluon matter in a magnetic field, Phys. At. Nucl. **76**, 1382 (2013).

[23] N. O. Agasian, Low-energy theorems of QCD and bulk viscosity at finite temperature and baryon density in a magnetic field, JETP Lett. **95**, 171 (2012).

[24] M. Kurian and V. Chandra, Bulk viscosity of a hot QCD medium in a strong magnetic field within the relaxation-time approximation, Phys. Rev. D **97**, 116008 (2018).

[25] K. Hattori and D. Satow, Electrical conductivity of quark-gluon plasma in strong magnetic fields, Phys. Rev. D **94**, 114032 (2016).

[26] A. Das, H. Mishra, and R. K. Mohapatra, Electrical conductivity and Hall conductivity of a hot and dense quark gluon plasma in a magnetic field: A quasiparticle approach, Phys. Rev. D **101**, 034027 (2020).

[27] M. Kurian, S. Mitra, S. Ghosh, and V. Chandra, Transport coefficients of hot magnetized QCD matter beyond the lowest Landau level approximation, Eur. Phys. J. C **79**, 134 (2019).

[28] M. Kurian and V. Chandra, Effective description of hot QCD medium in strong magnetic field and longitudinal conductivity, Phys. Rev. D **96**, 114026 (2017).

[29] A. Harutyunyan and A. Sedrakian, Electrical conductivity of a warm neutron star crust in magnetic fields, Phys. Rev. C **94**, 025805 (2016).

[30] B. O. Kerbikov and M. A. Andreichikov, Electrical conductivity of dense quark matter with fluctuations and magnetic field included, Phys. Rev. D **91**, 074010 (2015).

[31] S. i. Nam, Electrical conductivity of quark matter at finite T under external magnetic field, Phys. Rev. D **86**, 033014 (2012).

[32] S. Rath and B. K. Patra, Revisit to electrical and thermal conductivities, Lorenz and Knudsen numbers in thermal QCD in a strong magnetic field, Phys. Rev. D **100**, 016009 (2019).

[33] A. Das, H. Mishra, and R. K. Mohapatra, Electrical conductivity and Hall conductivity of a hot and dense hadron gas in a magnetic field: A relaxation time approach, Phys. Rev. D **99**, 094031 (2019).

[34] A. Bandyopadhyay, S. Ghosh, R. L. S. Farias, J. Dey, and G. Krein, Anisotropic electrical conductivity of magnetized hot quark matter, Phys. Rev. D **102**, 114015 (2020).

[35] L. Thakur and P. K. Srivastava, Electrical conductivity of a hot and dense QGP medium in a magnetic field, Phys. Rev. D **100**, 076016 (2019).

[36] B. Chatterjee, R. Rath, G. Sarwar, and R. Sahoo, Centrality dependence of electrical and Hall conductivity at RHIC and LHC energies for a conformal system, Eur. Phys. J. A **57**, 2 (2021).

[37] M. Kurian, Thermal transport in a weakly magnetized hot QCD medium, Phys. Rev. D **102**, 014041 (2020).

[38] K. Tuchin, Initial value problem for magnetic fields in heavy ion collisions, Phys. Rev. C **93**, 014905 (2016).

[39] A. Y. Potekhin, Electron conduction in magnetized neutron star envelopes, Astron. Astrophys. **351**, 787 (1999).

[40] P. Braun-Munzinger, K. Redlich, and J. Stachel, Particle production in heavy ion collisions, in *QuarkGluon Plasma 3* (World Scientific, 2004), pp. 491–599.

[41] E. M. Lifshitz and L. P. Pitaevskii, *Physical Kinetics* (Pergamon, Oxford, 1987).

[42] G. Endrődi, QCD equation of state at nonzero magnetic fields in the hadron resonance gas model, J. High Energy Phys. 04 (2013) 023.

[43] M. G. de Paoli and D. P. Menezes, Adv. High Energy Phys. (2014) 479401.

[44] G. S. Bali, F. Bruckmann, G. Endrődi, S. D. Katz and A. Schäfer, The QCD equation of state in background magnetic fields, J. High Energy Phys. 08 (2014) 177.